The Fornax3D project: intrinsic correlations between orbital properties and the stellar initial mass function

Poci, A.; McDermid, R.M.; Lyubenova, M.; Martín-Navarro, I.; Ven, G. van de; Coccato, L.; ... ; Zhu, L.

Monthly Notices of the ROYAL ASTRONOMICAL SOCIETY

MNRAS **514,** 3660–3669 (2022) https://doi.org/10.1093/mnras/stac1514
Advance Access publication 2022 June 7

The Fornax3D project: intrinsic correlations between orbital properties and the stellar initial mass function

A. Poci [1,2★] R. M. McDermid,[2,3] M. Lyubenova [4] I. Martín-Navarro,[5,6] G. van de Ven [7] L. Coccato [4] E. M. Corsini [8,9] K. Fahrion [10] J. Falcón-Barroso,[5,6] D. A. Gadotti [4] E. Iodice,[11] F. Pinna,[12] M. Sarzi,[13,14] P. T. de Zeeuw[15,16] and L. Zhu [17]

[1]*Centre for Extragalactic Astronomy, University of Durham, Stockton Road, Durham DH1 3LE, UK*
[2]*Research Centre for Astronomy, Astrophysics, and Astrophotonics, Department of Physics and Astronomy, Macquarie University, NSW 2109, Australia*
[3]*ARC Centre of Excellence for All Sky Astrophysics in 3 Dimensions (ASTRO 3D), Australia*
[4]*European Southern Observatory, Karl-Schwarzschild-Straße 2, D-85748 Garching bei München, Germany*
[5]*Instituto de Astrofísica de Canarias, Calle Via Láctea s/n, E-38205 La Laguna, Tenerife, Spain*
[6]*Departamento de Astrofísica, Universidad de La Laguna, E-38205 La Laguna, Tenerife, Spain*
[7]*Department of Astrophysics, University of Vienna, Türkenschanzstraße 17, A-1180 Wien, Austria*
[8]*Dipartimento di Fisica e Astronomia 'G. Galilei', Università di Padova, vicolo dell'Osservatorio 3, I-35122 Padova, Italy*
[9]*INAF - Osservatorio Astronomico di Padova, vicolo dell'Osservatorio 5, I-35122 Padova, Italy*
[10]*European Space Agency, European Space Research and Technology Centre, Keplerlaan 1, NL-2200 AG Noordwijk, the Netherlands*
[11]*INAF Osservatorio Astronomico di Capodimonte, via Moiariello 16, I-80131 Napoli, Italy*
[12]*Max-Planck-Institut für Astronomie, Königstuhl 17, D-69117 Heidelberg, Germany*
[13]*Armagh Observatory and Planetarium, College Hill, Armagh BT61 9DG, UK*
[14]*Centre for Astrophysics Research, University of Hertfordshire, College Lane, Hatfield AL10 9AB, UK*
[15]*Sterrewacht Leiden, Leiden University, Postbus 9513, NL-2300 RA Leiden, the Netherlands*
[16]*Max-Planck-Institut für Extraterrestrische Physik, Gießenbachstraße 1, D-85748 Garching bei München, Germany*
[17]*Shanghai Astronomical Observatory, Chinese Academy of Sciences, 80 Nandan Road, 200030 Shanghai, China*

Accepted 2022 May 25. Received 2022 May 24; in original form 2022 January 18

ABSTRACT

Variations of the stellar initial mass function (IMF) in external galaxies have been inferred from a variety of independent probes. Yet the physical conditions causing these variations remain largely unknown. In this work, we explore new spatially resolved measurements of the IMF for three edge-on lenticular galaxies in the Fornax cluster. We utilize existing orbit-based dynamical models in order to fit the new IMF maps within an orbital framework. We find that, within each galaxy, the high-angular momentum disc-like stars exhibit an IMF which is rich in dwarf stars. The centrally concentrated pressure-supported orbits exhibit similarly dwarf-rich IMF. Conversely, orbits at large radius which have intermediate angular momentum exhibit IMF which are markedly less dwarf-rich relative to the other regions of the same galaxy. Assuming that the stars which reside, in the present-day, on dynamically hot orbits at large radii are dominated by accreted populations, we interpret these findings as a correlation between the dwarf-richness of a population of stars, and the mass of the host in which it formed. Specifically, deeper gravitational potentials would produce more dwarf-rich populations, resulting in the relative deficiency of dwarf stars which originated in the lower mass accreted satellites. The central and high-angular momentum populations are likely dominated by *in situ* stars, which were formed in the more massive host itself. There are also global differences between the three galaxies studied here, of up to $\sim$0.3 dex in the IMF parameter ξ. We find no local dynamical or chemical property which alone can fully account for the IMF variations.

Key words: galaxies: elliptical and lenticular, cD – galaxies: evolution – galaxies: formation – galaxies: kinematics and dynamics – galaxies: star formation – galaxies: stellar content .

1 INTRODUCTION

The stellar initial mass function (IMF) is of paramount importance to many fields of astrophysics. Originally conceived as the probability distribution function of a local star formation episode as a function of stellar mass (though see Kroupa & Jerabkova 2019, for alternative interpretations), the IMF has a fundamental role across all scales of astrophysics. From star formation in individual giant molecular clouds (GMC), to galaxy formation, and subsequently, the assembly of structure in the Universe on large scales, the (potentially redshift-dependent) IMF has an impact across a broad range of physical and temporal scales. The IMF has direct implications for chemical yields from stellar evolution and chemical evolution on galactic scales (e.g.

★ E-mail: adriano.poci@durham.ac.uk

Yan, Jerabkova & Kroupa 2020), so an accurate IMF is critical to test models of those processes.

Despite its importance for extragalactic measurements, the vast majority of work on external galaxies is under the assumption of a constant IMF; between galaxies, within galaxies, or both. This is primarily driven by technical and fundamental limitations associated with *measuring* the IMF – especially for external galaxies. Yet indirect methods have provided mounting evidence of variations of the IMF between individual galaxies, and typically with some dependence on integrated galactic properties, such as the velocity dispersion (Treu et al. 2010; Thomas et al. 2011; Cappellari et al. 2012; La Barbera et al. 2013; Spiniello et al. 2014; Tortora et al. 2014; Posacki et al. 2015; Li et al. 2017; Rosani et al. 2018), α-element enrichment (Conroy & van Dokkum 2012b; McDermid et al. 2014), or total metal enrichment (Martín-Navarro et al. 2015c).

With increasingly modern data and measurement techniques, it is also becoming increasingly clear that the variations of IMF are local and correlate with local galactic properties. This is beginning to be exploited already by improved analysis techniques. Using spatially resolved data, gravity-sensitive spectral features – which provide constraints on the relative abundance of low-mass stars, which in turn is related to the slope of the IMF – are observed to vary with galactocentric radius, becoming relatively dwarf-rich at low radius (Martín-Navarro et al. 2015a, b; La Barbera et al. 2016; van Dokkum et al. 2017). In a similar analysis, Parikh et al. (2018) find similar radial trends – increasing dwarf-richness with decreasing radius – and an additional stellar mass dependence of that radial trend. They find, however, that using only the Wing-Ford FeH gravity-sensitive absorption feature produces the inverse radial behaviour, highlighting the observational difficulties associated with constraining the IMF. Sarzi et al. (2018) also found increasing dwarf-richness with decreasing radius with an abundance analysis of the nearby massive galaxy M 87 (NGC 4486). La Barbera et al. (2019) find that radius and surface mass density exhibit the strongest correlations with gravity-sensitive spectral features, even compared to the velocity dispersion.

Providing orthogonal constraints to gravity-sensitive absorption feature analyses, the discrepancy between dynamical and stellar masses (for a given IMF), the so-called IMF mismatch parameter $\alpha_{\rm IMF}$, is interpreted as a measure of the IMF, provided the dark matter can be accurately taken into account. Variations in this parameter are seen as evidence for a non-universal IMF both between and within galaxies (e.g. Cappellari et al. 2012; Lyubenova et al. 2016; Li et al. 2017; Oldham & Auger 2018). Using molecular gas as a high-spatial-resolution tracer of the gravitational potential (dynamical mass) in the central regions of a sample of nearby galaxies, Davis & McDermid (2017) find that this discrepancy can correlate positively, negatively, or not at all with galactocentric radius. They also report no correlations with other galactic properties, global or local.

The emphasis in recent times has been on the development of statistically robust methods, increasingly exploiting Bayesian techniques. This was motivated by the large number of free parameters of increasingly complex models, as well as the need to characterize potential correlations between them. In the specific case of the IMF, this approach has had a number of implementations. These include `alf` (Conroy & van Dokkum 2012a; Conroy, Graves & van Dokkum 2013; Conroy, van Dokkum & Villaume 2017), `PyStaff` (Vaughan et al. 2018), and 'Full-Index Fitting' (FIF; Martín-Navarro et al. 2019). This additional statistical constraining power comes with a marked increase in computational cost, so most of these techniques are restricted to coarse radial bins rather than taking advantage of the truly spatially resolved Integral-Field Unit (IFU) data (though see below).

While this transition from global to local correlations of the IMF represents a dramatic improvement in extragalactic IMF studies, the physical cause of these correlations remains elusive. Understanding what drives radial variations of the IMF has been challenging due to the vast array of galactic properties which also vary with radius, in particular, in the massivee early-type galaxies (ETG) which are most often the focus of extragalactic IMF studies. Unlike its global counterpart, the local velocity dispersion has been shown to be a poor predictor of the local IMF (e.g. Martín-Navarro et al. 2015c; Barbosa et al. 2021). Metallicity is key property believed to impact the IMF, and it often exhibits qualitatively similar (radially declining) gradients as observed for the IMF. However, the direct link between metallicity and IMF is not so clear; the correlation exhibits significant scatter and may be different for individual galaxies (Martín-Navarro et al. 2021). Moreover, metallicity variations alone cannot account for the observed IMF variations (e.g. Martín-Navarro et al. 2015c, 2021; McConnell, Lu & Mann 2016; Villaume et al. 2017). As such, it remains unclear with which galactic properties the IMF fundamentally varies.

Evidently these measurements require detailed modelling across the parameter-space of galactic properties in order to uncover drivers of this variation. In this work, we build upon the results of the Fornax3D survey, which has presented spatially resolved maps of the stellar IMF for quiescent galaxies in the survey (Martín-Navarro et al. 2021), as well as a qualitative connection between the structures of the projected IMF maps and the projected orbital components (Martín-Navarro et al. 2019). In this work, we apply a powerful orbit-based population-dynamical model to the FIF method for measuring the variations of the IMF across individual galaxies. By reproducing the measured IMF maps using our orbital dynamical model, we aim to investigate quantitative correlations of the local intrinsic kinematics with the local IMF.

2 DATA AND MODELS

In this work, we make direct use of the data and analysis presented in Poci et al. (2021, hereafter P21). That work studied three lenticular galaxies – FCC 153, FCC 170, and FCC 177 – using spectroscopic data from the Fornax3D survey (Sarzi et al. 2018) and photometric data from the Fornax Deep Survey (FDS; Iodice et al. 2016; Venhola et al. 2018). These galaxies are ideal because their nearly edge-on projection minimizes any uncertainty in analysing the various galactic components. Stellar kinematics were measured by extracting the first 6 Gauss-Hermite coefficients of the line-of-sight velocity distribution (LOSVD), fitting the observed spectra with the MILES empirical stellar library (Sánchez-Blázquez et al. 2006; Falcón-Barroso et al. 2011) in the `pPXF` (Cappellari & Emsellem 2004; Cappellari 2017) PYTHON package.[1] Stellar populations (ages, metallicities, and stellar mass-to-light ratios) were measured by fitting the observed spectra with the E-MILES single stellar population (SSP) library (Vazdekis et al. 2016), varying in age and metallicity for a fixed Kroupa (2002) IMF, again using `pPXF`. The analysis of these data comprised of Schwarzschild orbit-based dynamical models (using a general triaxial implementation; van de Ven, De Zeeuw & Van Den Bosch 2008; van den Bosch et al. 2008),[2] and the

[1] Available at https://pypi.org/project/ppxf/.

[2] We confirmed that the issues reported in Quenneville, Liepold & Ma (2022) do not affect our best-fitting models. We reran the model for FCC 170 and

self-consistent fitting of the measured stellar populations with these dynamical models.

Specifically, the best-fitting dynamical model for each galaxy was divided into a number of sub-components defined by their intrinsic kinematics properties. These properties are the orbital circularity, λ_z (Zhu et al. 2018), and the cylindrical time-averaged radius R. Each resulting sub-component has known intrinsic kinematic properties, and a known contribution to the original dynamical model. The projected mean stellar age and metallicity measured in P21 were then fit using this basis set of orbital components. This produced a model describing all measured stellar properties (kinematics, ages, and metallicities) within a single self-consistent orbital framework. We refer the reader to P21 for a full presentation of the dynamical model fits and related details. Here, we present the extension of this modelling approach to include an additional stellar-population property; namely, spatially resolved measurements of the stellar IMF.

3 MODELLING THE STELLAR POPULATIONS

3.1 Full-index fitting

Exploiting the parallel advances in computing technologies and observational instrumentation, Martín-Navarro et al. (2019) presented measurements which are sensitive to the relative fraction of low-mass stars. This is achieved by targeting specific absorption features that maximize the sensitivity to key parameters (including elemental abundances) while minimizing the computational overhead in fitting spectral pixel data. It is sufficiently computationally efficient that this measurement can be made for each spectrum in an IFU data-cube, and the IMF can therefore be investigated in a truly spatially resolved manner (not just radially).

The IMF in this instance is assumed to be a power law in stellar mass for high masses, and have a gradient of zero at low masses, following the functional form originally proposed by Vazdekis et al. (1996), and given here in equation (1).

$$\Phi(m) = \begin{cases} \beta\ 0.4^{-\Gamma_b}, & m/\mathrm{M}_\odot \leq 0.2 \\ \beta\ p(m), & 0.2 < m/\mathrm{M}_\odot < 0.6 \\ \beta\ m^{-\Gamma_b}, & m/\mathrm{M}_\odot \geq 0.6, \end{cases} \tag{1}$$

, where $p(m)$ is a spline ensuring a smooth transition between the two mass regimes, subject to the following boundary constraints:

$$\begin{aligned} p(0.2) &= 0.4^{-\Gamma_b} \\ \frac{\mathrm{d}p}{\mathrm{d}m}(0.2) &= 0 \\ p(0.6) &= 0.6^{-\Gamma_b} \\ \frac{\mathrm{d}p}{\mathrm{d}m}(0.6) &= -\Gamma_b\ 0.6^{-\Gamma_b - 1}. \end{aligned}$$

Population synthesis models are generated using this IMF, and the observed spectra are then compared with these models in order to make the measurements. Unlike conventional full-spectral fitting techniques, FIF isolates specific regions of a spectrum which contain IMF-sensitive information. In practice, this amounts to narrow band-passes surrounding key absorption features. FIF treats each spectral pixel along these absorption features as independent data points. This is therefore similar to full-spectral fitting, but without including the continuum regions between absorption features of the spectra.

Specifically, the Fe5270, Fe5335, Mg b5177, aTiO, TiO_1, and TiO_2 absorption features are modelled simultaneously to constrain the mean stellar age, metallicity, elemental abundances [α/Fe], and the high-mass power-law IMF slope Γ_b. The IMF is subsequently reparametrized in order to emphasize the changes in the stellar populations that are still directly observable in the present day. The specific parametrization utilized by FIF, and in this work, is defined as

$$\xi = \frac{\int_{m=0.2}^{0.5} \Phi\big[\log(m)\big]\ \mathrm{d}m}{\int_{m=0.2}^{1.0} \Phi\big[\log(m)\big]\ \mathrm{d}m} \tag{2}$$

$$= \frac{\int_{m=0.2}^{0.5} m \cdot X(m)\ \mathrm{d}m}{\int_{m=0.2}^{1.0} m \cdot X(m)\ \mathrm{d}m}, \tag{3}$$

where $\Phi[\log(m)]$ in equation (2) is the IMF in logarithmic mass units and $X(m)$ in equation (3) is the IMF in linear mass units.

ξ represents the ratio of low- to intermediate-mass stars. These mass ranges are expected to contribute to the observed spectrum of evolved galaxies, unlike higher mass stars which are likely to have evolved into non-luminous remnants by the present day. As presented in Martín-Navarro et al. (2019), literature IMF formalisms from Salpeter (1955), Kroupa (2002), and Chabrier (2003) have ξ values of 0.6370, 0.5194, and 0.4607, respectively. Note here that these values are derived using the functional forms specific to each of these three IMF, which all differ from the function used in this work given in equation (1). These values merely provide a relative scale by which to compare with the ξ measurements we observe in our sample. Larger values of ξ represent greater relative contributions from low-mass stars, producing more dwarf-rich populations.

The greater computational efficiency of FIF is achieved by excluding regions of the spectrum outside of specific absorption features. This does, in fact, reduce its ability to constrain the variations in different regions of the spectrum, and the continuum itself may also contain useful information. To circumvent this issue, an initial fit is performed on the full spectrum using a (non-Bayesian) quadratic solver – namely, `pPXF` – which provides a prior to the Bayesian fit for ages, metallicities, and abundances. Additionally, of the absorption features listed above, only [Mg/Fe] constrains the [α/Fe] abundances. The variations of other individual elemental abundances are coupled to the variations of the [Mg/Fe], further improving the efficiency at the cost of reduced generality. Maps of stellar population properties for all passive ETGs in the Fornax3D sample derived using FIF are presented in Martín-Navarro et al. (2021). Here, we use the derived maps of ξ from that work to build an orbit-based description of the IMF properties measured for our three-edge-on lenticular galaxies.

3.2 An orbital analysis of the IMF

The method presented in P21 allowed the detailed analysis of a galaxy's assembly history through the intrinsic properties it provides. It exploits the straight-forward principle that the observed data result from the integrated contributions of many distinct populations of stars through the line of sight (LOS). We apply the same concept here, this time with the IMF parameter ξ.

From dynamical models presented in P21, the orbits were bundled into distinct dynamical sub-components using the orbital $\lambda_z - R$ phase-space. While the same criterion for the phase-space bundling was applied to all three galaxies (see Poci et al. 2019, P21), the final set of sub-components depends on the specific phase-space distribution from the best-fitting Schwarzschild model of each individual galaxy. In the end, there are sets of 448, 455, and 449

confirmed that none of the best-fitting model parameters depart from the values presented in P21. A more thorough comparison is presented in Thater et al. (2022), showing that none of the physical properties of the models are significantly impacted, over a broad range of galaxy types and observational data.

distinct dynamical components with non-zero weights from the Schwarzschild models of FCC 153, 170, and 177, respectively. These numbers of phase-space components provide the required flexibility in physical space in order to reproduce the complex spatial variations in the projected stellar population maps.

The relative contribution (luminosity weight) from each sub-component/population i through the LOS in a given spatial bin is known via the decomposition of the orbital phase-space. There exists then a set of ξ^i which, when linearly combined with the pre-determined luminosity weights, reproduces the measured map of ξ. This framework is described by equation (4).

$$\begin{pmatrix} \tilde{\omega}_1^1 & \tilde{\omega}_1^2 & \cdots & \tilde{\omega}_1^{N_{\rm comp.}} \\ \tilde{\omega}_2^1 & \tilde{\omega}_2^2 & \cdots & \tilde{\omega}_2^{N_{\rm comp.}} \\ \vdots & \vdots & \ddots & \vdots \\ \tilde{\omega}_{N_{\rm aper}}^1 & \tilde{\omega}_{N_{\rm aper}}^2 & \cdots & \tilde{\omega}_{N_{\rm aper}}^{N_{\rm comp.}} \end{pmatrix} \cdot \begin{pmatrix} \xi^1 \\ \xi^2 \\ \vdots \\ \xi^{N_{\rm comp.}} \end{pmatrix} = \begin{pmatrix} \xi'_1 \\ \xi'_2 \\ \vdots \\ \xi'_{N_{\rm aper}} \end{pmatrix} \tag{4}$$

The $\tilde{\omega}$ represent the normalized luminosity weights for each dynamical sub-component, as defined in Section 2 (columns of the matrix), in each spatial aperture (rows of the matrix). The ξ^i represent the IMF parameter of each dynamical component $i \in [1, N_{\rm comp.}]$, and the ξ'_j represent the observed IMF parameter in each spatial aperture $j \in [1, N_{\rm aper.}]$. The ξ'_j are the observed values computed using the Γ_b measurements from FIF, as described in Section 3.1. We solve equation (4) for the set of ξ^i by inversion. The outcome of this process is that each dynamical component has a fitted ξ which is constrained by the IMF parameter measured with FIF, and consistent with the orbital weights derived from the prior fit to the observed kinematics. This process works by exploiting the consistent weighting between the observations and the models; the observed stellar kinematics (and therefore the Schwarzschild model) as well as the outputs from the FIF technique are all luminosity-weighted. This means that the effect of a given component's intrinsic kinematics on the observed spectrum (the shifting and/or broadening of lines) is captured by the relative weighting of that same component's LOSVD, as derived by the dynamical decomposition of the Schwarzschild phase-space. Therefore, the intrinsic combination of sub-populations through the LOS is reflected in both the spectra for FIF and the dynamical decomposition. This same concept, but for age and metallicity, was verified in P21.

Solving equation (4), which consists of a straight-forward non-negative linear matrix inversion, is done with a Bounded-Value Least Squares (BVLS) fit using the `lsq_linear` implementation within the SciPy ecosystem (Virtanen et al. 2020). Despite reducing the freedom of the model by grouping orbits in integral space into dynamical sub-components, there remains some level of degeneracy in the fit to the single map of mean ξ. To minimize the impact of this, we apply linear regularization to the solution weights, as described in detail in Poci et al. (2019). The regularization, in the case where two solutions fit the data equally well, will favour the solution which has the smoothest distribution in weight-space; in our case, in the $\lambda_z - R$ plane. In physical terms, orbits with similar angular momentum (λ_z) and (cylindrical) radius will preferentially be given similar values of ξ *if* such a solution is otherwise indistinguishable from one which varies more rapidly.

4 RESULTS

4.1 Fits to observational data

The results of the fits to the IMF parametrizations are presented in Figs 1 to 3, for FCC 153, FCC 170, and FCC 177, respectively. The

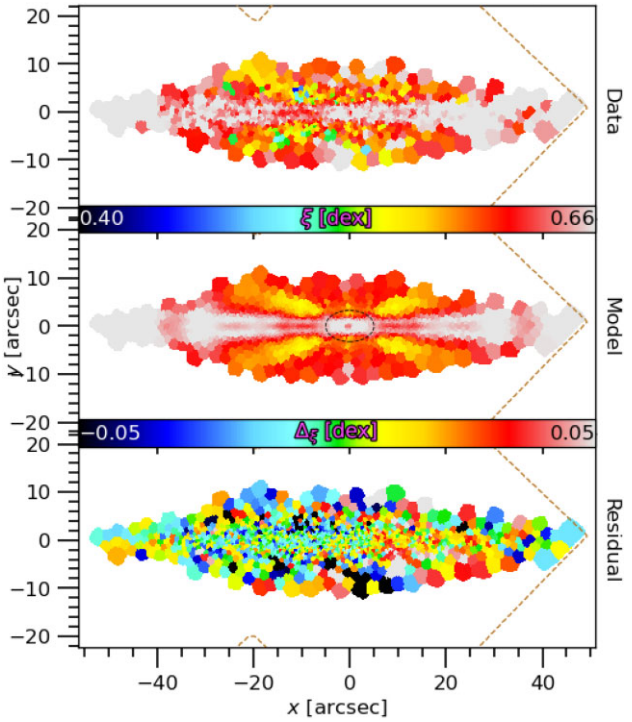

Figure 1. The IMF fit for FCC 153. From top to bottom, the maps show the data, model, and residuals (data-model). The outline of the MUSE mosaic is shown in dashed brown. The dashed black ellipse in the 'Model' panel illustrates the intrinsic radius which separates the 'outer' and 'inner' hot components as determined by the orbital phase-space (with ellipticity corresponding to the average ellipticity of the galaxy). Maps of ξ are presented on a common colour scale across all galaxies for comparison.

structures in the ξ maps do not necessarily follow those of the age and metallicity maps directly (luminosity-weighted measurements presented in P21). In FCC 153, ξ is noticeably elevated along the young, metal-rich disc. There is a minor central peak, but FCC 153 has a small (if any) central pressure-supported component, so a dramatic change in this region is not necessarily expected. In FCC 170, the IMF is seen to be dwarf-rich both in the relatively young disc and in the more metal-rich, old central component. Clearly, then, neither age nor metallicity alone can fully account for the IMF variation in FCC 170. Finally, in FCC 177, the IMF shows similar structure as the metallicity such that ξ is elevated along the disc and in a spheroidal-like central component. The exception is the very central region, embedded within the spheroid. This region appears to have a relatively high abundance of intermediate-mass stars (lower ξ). This feature is mirrored by significantly younger ages and lower M_*/L in this region, indicating a sudden shift in the time and conditions of that star formation episode. However, this region may be influenced by the young metal-rich nuclear star cluster in this galaxy (Fahrion et al. 2021).

4.2 The IMF in the circularity plane

The orbital framework we have used to fit the measured ξ maps allows us to investigate the distribution of IMF throughout each galaxy; specifically, correlations with intrinsic dynamical properties. In Figs 4 to 6, we reproject the circularity phase-space as a function of ξ. The transparency indicates the orbital weighting derived from the original Schwarzschild model. In these projections, regions with

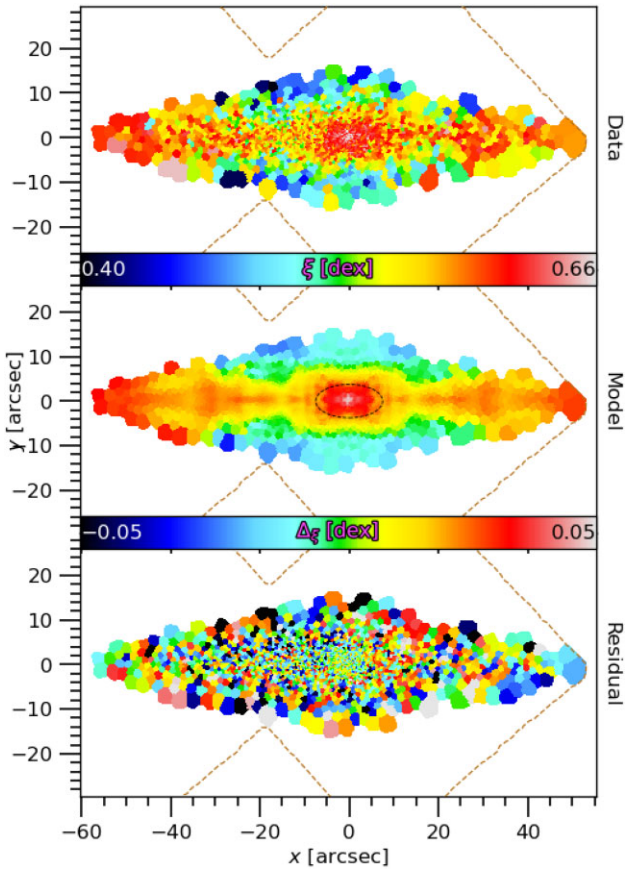

Figure 2. As Fig. 1, but for FCC 170.

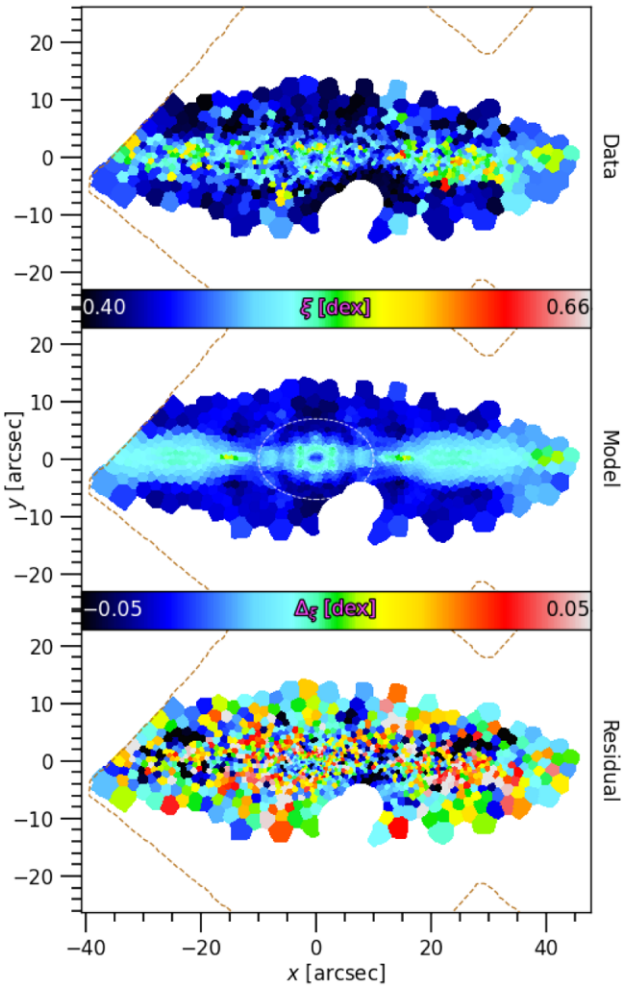

Figure 3. As Fig. 1, but for FCC 177.

low transparency do not contribute significantly to the models/maps, irrespective of the integrated value of ξ (colour) in that region.

These projections clearly illustrate the relative difference of ξ between galaxies (most notably with FCC 177). Internally, they also show that the dwarf-rich (high ξ) populations exist on orbits with high-angular momentum (λ_z) and/or are centrally concentrated. Conversely, the dynamically warm regions always exhibit relatively less dwarf-rich populations within each galaxy. These differences may be related to the origin of the stars in each component, discussed further in Section 5.

4.3 The IMF of principle galactic orbital components

Although many dynamical components were used to fit the observed ξ map, the dynamic range of the spatial variations in the case of the IMF are markedly reduced with respect to age and metallicity. As a result, we do not attempt a fine-grain dynamical decomposition of the IMF maps. Instead, we draw conclusions about the major dynamical structures expected in S0 galaxies in order to reduce the numerical noise of the fitting method caused by the relatively noisy observed IMF maps. To do this, we define a rotationally supported 'cold' component as having $\lambda_z \geq 0.8$. A single radial cut is applied to the remaining orbits with $\lambda_z < 0.8$ in order to isolate the central pressure-supported spheroid. This radius is derived from the original circularity phase-space by approximately identifying the natural ridge in the weight distributions given in P21 and illustrated by the transparency in Figs 4 to 6. This is 10 arcsec (1.0 kpc) for FCC 153, 15 arcsec (1.6 kpc) for FCC 170, and 20 arcsec (1.9 kpc) for FCC 177, reflecting the different dynamical configurations of the galaxies. These regions were previously identified as being bulge-dominated in Pinna et al. (2019a, b). We refer to these as the 'inner' and 'outer' hot components, respectively, in contrast to the 'cold' component which occupies all radii at the highest circularities. These components are shown in Figs 4 to 6 for reference, and we can now investigate their respective average IMF properties.

To quantitatively compare the dynamical components and galaxies, we compute the luminosity-weighted average ξ for each region demarcated in Figs 4 to 6. We show these averages in Fig. 7 as a function of the average circularity of the dynamical components. Specifically, for all orbits which satisfy the respective selection criteria of each dynamical component, we compute the average ξ weighting by the orbital luminosity weights from the original Schwarzschild model fit. Furthermore, to avoid being driven by orbits which are unconstrained by kinematics, all averages are computed for only those orbits within the spectroscopic field-of-view – that is, with time-averaged radius within the maximum spectroscopic extent $R_{\rm max}$.

Corroborating the conclusions from Section 4.2, Fig. 7 shows that each outer hot component is deficient in dwarf stars relative to the other regions in its host galaxy. Moreover, Fig. 7 clearly illustrates the absolute difference between FCC 177 and the other two galaxies. While our sample consists of three galaxies, the distribution of these galaxies in Fig. 7 is inconsistent with being driven by many of their

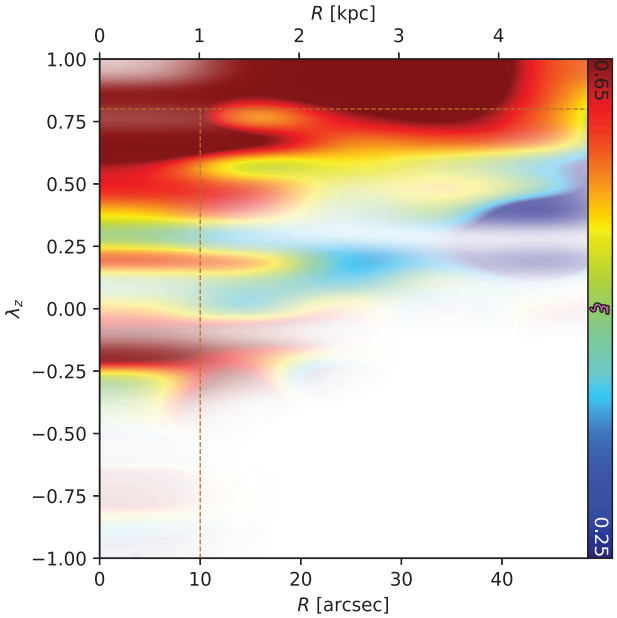

Figure 4. The circularity phase-space coloured by IMF for FCC 153. The colour bar, common to all three galaxies, shows the luminosity-weighted average ξ in each region. The original weight distribution of the underlying orbits is depicted by transparency, where opaque represents high weight and transparent represents zero weight. The brown dashed lines illustrate the dynamical selection of the three broad components explored in Section 4.3.

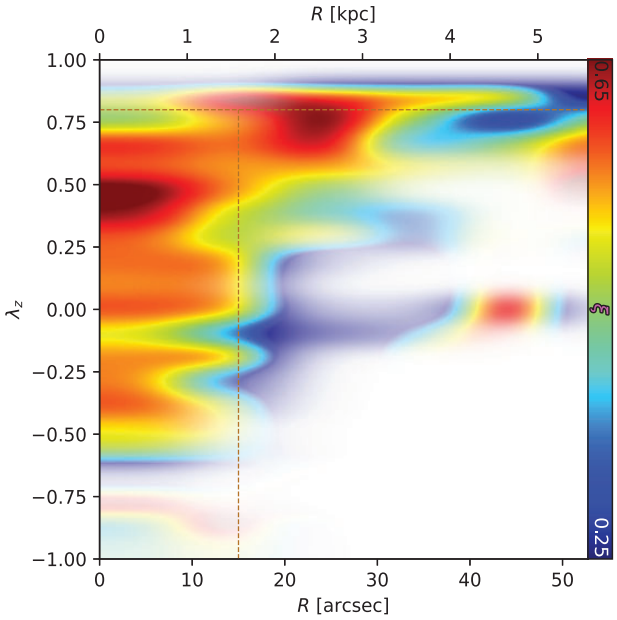

Figure 5. As Fig. 4, but for FCC 170.

present-day properties. ξ does not correlate with either the present-day projected cluster-centric distance or suspected time of in-fall into the cluster, which both increase from FCC 170 to FCC 153. This is in agreement with the lack of dependence of the IMF on environment found previously, for both galaxy-scale (Eftekhari et al. 2019) and local (Damian et al. 2021) environment. There is also no correlation with present-day stellar mass or central velocity dispersion, both increasing from FCC 177 to FCC 170. Local ξ clearly does not

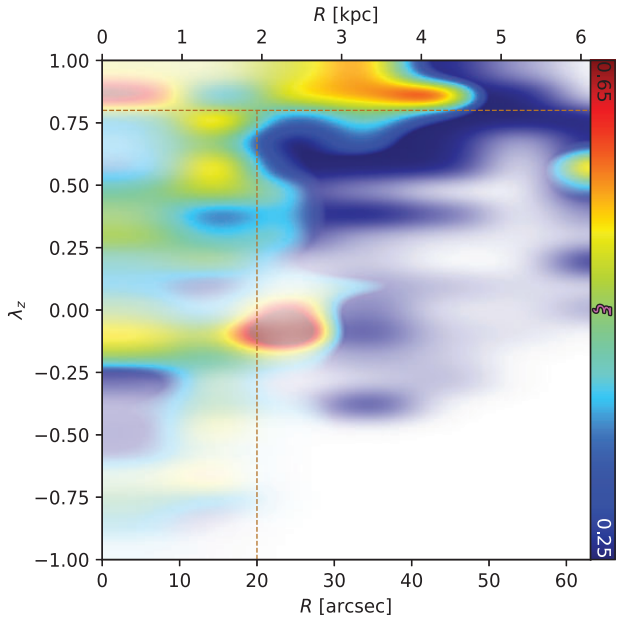

Figure 6. As Fig. 4, but for FCC 177.

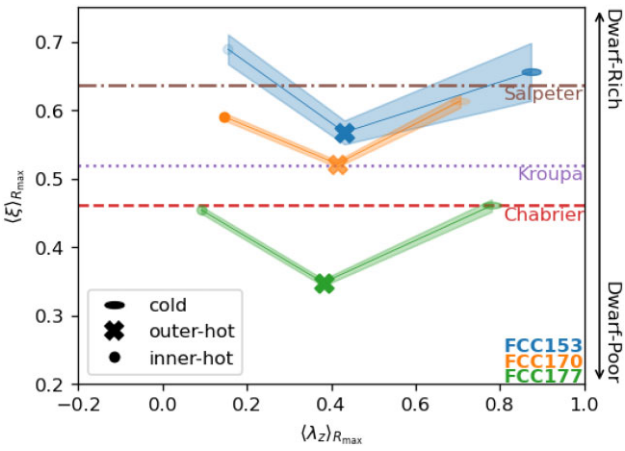

Figure 7. The luminosity-weighted average IMF as a function of the luminosity-weighted average orbital circularity for the three dynamical components (*symbols*, defined in text) of the three Fornax3D galaxies. Transparency of the symbols denotes the relative orbital weight of each dynamical component within a given galaxy, with opaque and transparent corresponding to high and low orbital weight, respectively. Horizontal lines mark literature IMF values for reference. Note that these reference values are computed using equation (3) given their respective IMF functions, which differ from that used in this work, defined in equation (1). Only those orbits with time-averaged radii within the spectroscopic data are included during the averaging. Relatively dwarf-rich populations are present in the cold and inner hot components. The outer hot populations are markedly more dwarf-poor relative to the others. FCC 177 globally exhibits relatively dwarf-poor populations compared to the other two galaxies.

correlate with the local orbital circularity, leading to the non-linear relation between the dynamical components of each galaxy in Fig. 7.

We finally explicitly explore the relationship between local metallicity and local IMF in Fig. 8. There does indeed exist a mild correlation between the local metallicity and local IMF, as found previously (e.g. Martín-Navarro et al. 2021), such that more dwarf-rich populations are favoured for higher mean stellar metallicity [as a

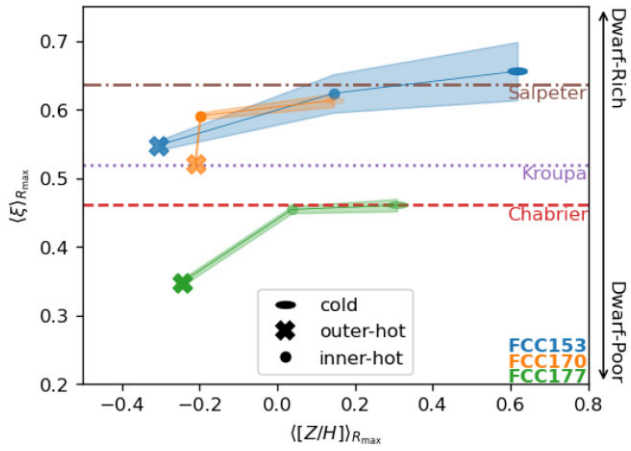

Figure 8. As Fig. 7, but for luminosity-weighted average metallicity.

proxy for the interstellar medium (ISM) metallicity at the time of star formation]. It cannot, however, account for all of the IMF variations seen even in these few galactic components. For instance, the disc and inner hot component of FCC 177 exhibit the same average IMF, but different metallicities. Conversely, the inner and outer hot components of FCC 170 exhibit similar average metallicities but different IMFs. This is unsurprising, given the large scatter in the metallicity–IMF correlations, especially at low metallicity (e.g. Martín-Navarro et al. 2015c; La Barbera et al. 2019).

5 DISCUSSION

5.1 The local variations of the galactic IMF

As seen from the results in Section 4, there appears to be no single galactic property which can account for the local variations of the IMF parameter. Instead, such variations are tied to the orbital structure of the host. This is unexpected from literature studies of IMF variations. There, the interpretation is usually that the 'extreme' conditions present in the central regions of massive elliptical galaxies (often highly pressure-supported) is what gives rise to these IMF variations (e.g. Sonnenfeld et al. 2012; Wegner et al. 2012; Dutton et al. 2013b; Spiniello et al. 2014; Martín-Navarro et al. 2015c; Smith et al. 2015). Moreover, there have only been a small number of studies in which the IMF is explored across galactic components. Dutton et al. (2013a) and Brewer et al. (2014) use strong lensing and gas dynamics to constrain the IMF of bulges and discs separately. They find that the bulges favour dwarf-rich IMF such as Salpeter (1955), and while the disc IMF are degenerate with the dark matter halo, they are more consistent with less dwarf-rich, Milky Way-like IMF such as Chabrier (2003).

We instead look to properties defining the conditions in which the stars are actually formed, since present-day structural components do not necessarily capture evolutionary changes experienced by the galaxy. In P21, one tentative conclusion was that FCC 170 and FCC 153 have accreted a similar amount of stellar mass, $\log_{10}(M_{\rm acc}/{\rm M}_{\odot}) \sim 9$, while for FCC 177 it is approximately 1 dex lower. Specifically, for FCC 170 it is claimed to have been brought in by a higher number of lower mass satellites in order to explain the lower metallicity of the warm orbital families, compared to fewer higher mass satellites for FCC 153. These accreted populations would reside predominately in the outer hot components (e.g. Monachesi et al. 2019; Davison et al. 2021). If that is indeed the case, we may posit that the galaxy mass and/or ISM metallicity *at the time of star formation* could be the driver of these uncovered IMF trends, such that stars formed in the lower mass/lower metallicity progenitors contribute relatively dwarf-deficient populations to the present-day hosts. For FCC 177, being overall lower mass, this explains the global shift to less dwarf-rich populations in both the *in situ* (cold and inner hot) and *ex situ* (outer hot) components. Additionally, the offset of the outer hot component of FCC 170 towards less dwarf-rich populations with respect to that of FCC 153 in Fig. 7 would be explained by the suspected lower mass satellites accreted on to the former.

While investigating the role of turbulence in setting the slope of the IMF, Nam, Federrath & Krumholz (2021) find that more shallow power spectra of turbulence result in more shallow high-mass IMF slopes. That is, they find that relatively lower power in large-scale turbulence correlates with relatively higher contributions from high-mass stars. Chabrier, Hennebelle & Charlot (2014) similarly find that in highly dense and turbulent environments, the peak of the IMF is shifted towards lower stellar masses, implying relatively higher contributions from low-mass stars. Should lower mass galaxies have lower power in large-scale turbulence, this result would imply that they should have more shallow IMF slopes compared to higher mass galaxies with relatively larger power in large-scale turbulence, supporting the results of our models. Interestingly, Dutta et al. (2013) find only a weak relation between the dynamical mass (and H I mass) of spiral galaxies and the index of the power spectrum of turbulence, for dynamical masses between $\sim 10^{11}$ and 10^{12} M$_{\odot}$. However, that sample covers a relatively small range of dynamical masses, so may not be conclusive. Potentially a more comprehensive sample would reveal any correlations between the dynamical mass of galaxies, the resulting turbulence of their ISM, and the subsequent impact on the dwarf-richness of the stars formed there.

Related, or perhaps alternatively, to turbulence, metallicity has been seen to clearly correlate with the IMF, both globally (e.g. Martín-Navarro et al. 2015c) and locally (e.g. Feldmeier-Krause, Lonoce & Freedman 2021). Our results in Fig. 8 are qualitatively consistent with those of Marks et al. (2012) and the galaxy-wide IMF of Yan, Jeřábková & Kroupa (2021), though we find that metallicity alone cannot fully explain the IMF variations. It is well-known that metallicity (both gaseous and stellar) correlates with mass (e.g. Tremonti et al. 2004; Gallazzi et al. 2005; Gao et al. 2018; Curti et al. 2020). However, recent evidence suggests that it is actually the average gravitational potential which drives these correlations rather than mass (Barone et al. 2018; D'Eugenio et al. 2018, using $M_{\star}/R_{\rm e}$ as an observational proxy to the gravitational potential), corroborated by correlations between average metallicity and central velocity dispersion (e.g. McDermid et al. 2015). The connection between the dwarf-richness of a population and the present-day gravitational potential of its host has already been proposed (van Dokkum & Conroy 2012). However, this observational correlation would be 'polluted' by the varying (and unknown) contributions from *ex situ* populations in observed galaxies. An ideal test would require distinct accretion events to be identified and separated in both their IMF and metallicity distributions. Conversely, Nipoti et al. (2020) find that dry minor mergers in massive ETG flatten existing gradients of $\alpha_{\rm IMF}$, but they claim this is predominantly due to mixing of populations, rather than differences in the original populations of each progenitor galaxy.

The results of the literature works on massive elliptical galaxies are usually interpreted as being facilitated specifically by the conditions in the centres of galaxies, supporting the overabundance of low-mass stars. However, by definition, these elliptical galaxies do not have any significant disc structure. Owing to their structural symmetry,

the IMF is therefore studied radially, typical of gradients in other properties of ETG. Those galaxies also have the largest accretion fractions on average (Oser et al. 2010; Khochfar et al. 2011; Lackner et al. 2012; Rodriguez-Gomez et al. 2016). Therefore, taken in the context of the results of this work, it is possible that the central regions of those massive ellipticals are dwarf-rich because they likely formed *in situ* in a relatively massive halo, while the exteriors are less dwarf-rich because their stars were formed in, then accreted from, lower mass systems. This leads to a shift in the interpretation of local galactic IMF variations from being caused by the 'extreme' conditions at the centres of massive elliptical galaxies, to being determined by the origins of the stars themselves, likely depending on the mass of the system in which they were formed. In present-day galaxies, IMF variations are, in this scenario, explained by the mixing of *in situ* and *ex situ* populations whereby the stars are formed in a variety of host masses.

In absolute terms, the cold components measured here are significantly dwarf-rich, being consistent with a Salpter-like IMF for FCC 153 and FCC 170. This is comparable to the central regions of the massive ETG studied previously (e.g. Sonnenfeld et al. 2012; Wegner et al. 2012; Dutton et al. 2013a; Shetty & Cappellari 2014; Oldham & Auger 2018), as well as the centres of a handful of other galaxies in the Fornax cluster (Martín-Navarro et al. 2021), despite the significant physical differences in the galaxy types, densities, and internal kinematics. However, IMFs with 'super-Salpeter' concentrations of dwarf stars have been seen in some of the most massive galaxies (e.g. Tortora, Romanowsky & Napolitano 2013; Spiniello et al. 2014; Smith et al. 2015; Conroy et al. 2017), consistent with the idea that the gravitational potential in which the stars form is at least partially responsible for the level of dwarf-richness. Conversely, FCC 177 exhibits markedly less dwarf-rich populations globally, and especially in its outer hot region. FCC 177 has, however, had a significantly more extended and delayed star-formation history, and it is also the lowest mass, compared to the other two Fornax galaxies (P21).

In reality, the gravitational potential at birth is not likely the sole driver of observed IMF variations. There are, for instance, variations observed in galaxies expected to have experienced effectively no accretion (Ferré-Mateu et al. 2017). More likely, dwarf-rich populations could be favoured in a more metal-rich ISM at fixed gravitational potential (explaining the observed metallicity – IMF correlations and its large scatter), or deeper gravitational potentials at fixed ISM metallicity (explaining the deficiency of low-mass stars in the outer hot components in Fig. 7), at the time of star formation. But directly measuring such a correlation from observations would require both a detailed str-formation history in order to measure the historic mass and metallicity of the host galaxy during each episode of star formation, as well as timing every accretion event which has occurred in its assembly history.

5.2 IMF parametrizations

There are a number of functional forms for the IMF presented in the literature. In addition to that of Vazdekis et al. (1996), other smooth functions have been proposed (e.g. Miller & Scalo 1979; Chabrier 2003), while many studies utilize generic power laws with varying levels of flexibility in the slopes (e.g. Kroupa 2002; Conroy et al. 2017; Conroy et al. 2018; van Dokkum et al. 2017; Vaughan et al. 2018; Lonoce, Feldmeier-Krause & Freedman 2021). Moreover, for a given functional form, the IMF may be parametrized in any number of ways, with dwarf-to-giant ratios being frequently used (e.g. La Barbera et al. 2013; Lyubenova et al. 2016). In this work, we have used a single parametrization (ξ) of a single functional form (Vazdekis et al. 1996).

Although Γ_b is measured directly from the spectra via FIF, we do not use it in the orbital fitting. Γ_b describes the slope of an abstract mass distribution, and therefore does not satisfy the linearity requirements of equation (4). That is, for an integrated population through the LOS consisting of k sub-populations with Γ_b^k, the slope of the integrated IMF is not given simply by the weighted average over all Γ_b^k, because Γ_b responds non-linearly to changes in the mass function. Since equation (4) is set up to compute the average through the LOS, Γ_b is unsuitable for this fitting process. Conversely, ξ represents a physical mass fraction, and thus the mass fraction of the total population is indeed given by the weighted average over its sub-populations. It is for this reason that ξ is used throughout this work.

For a given functional form of the IMF, Γ_b and ξ uniquely map to one another. However, different functional forms could produce the same ξ value with different characteristic slopes. This means that the precise translation from ξ to Γ_b (or indeed from ξ to specific spectral responses) is sensitive to the assumed form of the IMF. The main results of this work focus on the *relative* abundance of low-mass stars between dynamical components within galaxies for a given form of the IMF. However, comparisons to other results and literature IMF are subject to the assumption that the response of a spectrum for a given ξ value is the same for different IMF functions.

5.3 Further developments

One implication of Fig. 7 is that the greatest internal variations of IMF are in the 'warm' components. These components reside in the diffuse outer regions, where there is limited coverage by the IFU data. Larger radial coverage of these galaxies will strengthen the results of this work, as the fraction of accreted material is expected to be higher at larger radius (for instance, Karademir et al. 2019). Further extending the IFU mosaic with additional (though necessarily deeper) observations, in particular along the minor axis, would also improve coverage of this important *ex situ* material.

Broadly, our results indicate that both local and global galactic properties influence the IMF. In addition to those presented in P21, we have found further independent evidence that the present-day orbits of stars retain information about their respective star formation conditions, in this case encoded in their IMF. Larger samples of galaxies are certainly needed for more robust conclusions. If indeed the gravitational potential at the time of star formation is what determines the IMF, a targeted sample of so-called relic galaxies (Beasley et al. 2018) spanning a range of stellar mass to which we apply our methodology could in principle provide the necessary test of this hypothesis. This is because relic galaxies are suspected to have had little-to-no accretion to the present day, which removes the uncertainty of measuring and timing the accretion events in a galaxy's assembly history. Incidentally, such a sample is currently being compiled (Spiniello et al. 2021), however, without sufficient spatial resolution to conduct the orbital analysis developed here. Independently, a sample in field environments mass-matched to the Fornax galaxies studied here would also be ideal to probe any potential effects from the cluster environment which may be present in the current results.

This implementation has enabled the direct comparison between the local orbital structure and stellar IMF for external galaxies. Our developments in fact pre-date the means to strictly verify them, as no current cosmological simulations can model the complexity of variable IMF – though this is beginning to change with one

recent instance which includes preliminary IMF treatments (Barber, Crain & Schaye 2018). While isolated simulations have been performed incorporating non-universal IMF (Bekki 2013), testing our methodology on these simulations would only assess its accuracy in numerically recovering known input quantities – which has already been shown in Zhu et al. (2020) and P21. Thus, a more physically motivated investigation of how accurately genuine IMF variations can be recovered within this orbital framework will require the advent of more sophisticated models for star formation in future cosmological simulations.

6 CONCLUSIONS

This work has presented the first investigation of direct correlations between intrinsic local orbital properties and local stellar IMF. Using an orbit-based dynamical model of the stellar kinematics, we have reproduced the spatially resolved observed maps of the stellar IMF. We then investigated how the stellar IMF depends on the intrinsic angular momentum λ_z. We find that the relative abundance of dwarf stars, parametrized by ξ, is higher in both the high-angular momentum ('disc') and central pressure-supported ('bulge') orbits, while being markedly lower in the outer pressure-supported ('accreted inner halo') orbits. We interpret this relationship as being driven – at least partially – by the mass of the progenitor systems in which the stars formed, with lower mass galaxies preferentially forming with lower relative abundance of low-mass stars. In this scenario, the variations of the IMF observed in our sample of external galaxies in the present day is caused by the variations in individual assembly histories. This subsequently leads to a variety of *in situ*-to-*ex situ* population mixtures, where different populations were formed in progenitor systems of different mass and contribute different IMF to the galaxy observed in the present day.

This analysis has presented an alternative interpretation of existing IMF results, which had inferred that significant IMF variations are only the result of extreme conditions in the most massive galaxies. We instead propose a scenario in which the IMF of a given population is determined by the level of turbulence supported by the gravitational potential of its host galaxy at the time of star formation, and that accretion/assembly processes can impose internal structure in the distribution of IMF properties within galaxies. Testing this hypothesis will require a dedicated sample of galaxies, likely facilitated by next-generation observational facilities, and/or highly detailed simulations resolving the hydrodynamical effects on roughly parsec scales.

ACKNOWLEDGEMENTS

Based on observations collected at the European Southern Observatory under ESO programme 296.B-5054(A). AP was supported by the Science and Technology Facilities Council through the Durham Astronomy Consolidated Grant 2020-2023 (ST/T000244/1). RMcD acknowledges financial support as a recipient of an Australian Research Council Future Fellowship (project number FT150100333). IM-N and JF-B acknowledge support through the RAVET project by the grant PID2019-107427GB-C32 from the Spanish Ministry of Science, Innovation and Universities (MCIU), and through the IAC project TRACES which is partially supported through the state budget and the regional budget of the Consejería de Economía, Industria, Comercio y Conocimiento of the Canary Islands Autonomous Community. GvdV acknowledges funding from the European Research Council (ERC) under the European Union's Horizon 2020 research and innovation programme under grant agreement number 724857 (Consolidator Grant ArcheoDyn). EMC acknowledges support by Padua University grants DOR1885254/18, DOR1935272/19, and DOR2013080/20 and by Italian Ministry for Education University and Research (MIUR) grant PRIN 2017 20173ML3WW_001. FP acknowledges support from grant PID2019-107427GB-C32 from The Spanish Ministry of Science and Innovation. Finally, we thank the anonymous referee for their detailed comments, which have improved the clarity of this work.

This work makes use of the `SciGar` compute cluster at ESO, and the `OzStar` supercomputer at Swinbourne University. The work also makes use of existing software packages for data analysis and presentation, including AstroPy (Astropy Collaboration et al. 2013), Cython (Behnel et al. 2011), IPython (Perez & Granger 2007), matplotlib (Hunter 2007), NumPy (Harris et al. 2020), the SciPy ecosystem (Virtanen et al. 2020), and statsmodels (Seabold & Perktold 2010).

DATA AVAILABILITY

No new data were generated or analysed in support of this research.

REFERENCES

Astropy Collaboration, 2013, A&A, 558, A33
Barber C., Crain R. A., Schaye J., 2018, MNRAS, 479, 5448
Barbosa C. E., Spiniello C., Arnaboldi M., Coccato L., Hilker M., Richtler T., 2021, A&A, 649, A93
Barone T. M. et al., 2018, ApJ, 856, 64
Beasley M. A., Trujillo I., Leaman R., Montes M., 2018, Nature, 555, 483
Behnel S., Bradshaw R., Citro C., Dalcin L., Seljebotn D. S., Smith K., 2011, Comput. Sci. Eng., 13, 31
Bekki K., 2013, MNRAS, 436, 2254
Brewer B. J., Marshall P. J., Auger M. W., Treu T., Dutton A. A., Barnabè M., 2014, MNRAS, 437, 1950
Cappellari M., 2017, MNRAS, 466, 798
Cappellari M., Emsellem E., 2004, PASP, 116, 138
Cappellari M. et al., 2012, Nature, 484, 485
Chabrier G., 2003, PASP, 115, 763
Chabrier G., Hennebelle P., Charlot S., 2014, ApJ, 796, 75
Conroy C., van Dokkum P., 2012a, ApJ, 747, 69
Conroy C., van Dokkum P. G., 2012b, ApJ, 760, 71
Conroy C., Graves G. J., van Dokkum P. G., 2013, ApJ, 780, 33
Conroy C., van Dokkum P. G., Villaume A., 2017, ApJ, 837, 166
Conroy C., Villaume A., van Dokkum P. G., Lind K., 2018, ApJ, 854, 139
Curti M., Mannucci F., Cresci G., Maiolino R., 2020, MNRAS, 491, 944
D'Eugenio F., Colless M., Groves B., Bian F., Barone T. M., 2018, MNRAS, 479, 1807
Damian B., Jose J., Samal M. R., Moraux E., Das S. R., Patra S., 2021, MNRAS, 504, 2557
Davis T. A., McDermid R. M., 2017, MNRAS, 464, 453
Davison T. A., Norris M. A., Leaman R., Kuntschner H., Boecker A., van de Ven G., 2021, MNRAS, 507, 3089
Dutta P., Begum A., Bharadwaj S., Chengalur J. N., 2013, New Astron., 19, 89
Dutton A. A. et al., 2013a, MNRAS, 428, 3183
Dutton A. A., Macciò A. V., Mendel J. T., Simard L., 2013b, MNRAS, 432, 2496
Eftekhari E., Mosleh M., Vazdekis A., Tavasoli S., 2019, MNRAS, 486, 3788
Fahrion K. et al., 2021, A&A, 650, A137
Falcón-Barroso J., Sánchez-Blázquez P., Vazdekis A., Ricciardelli E., Cardiel N., Cenarro A. J., Gorgas J., Peletier R. F., 2011, A&A, 532, A95
Feldmeier-Krause A., Lonoce I., Freedman W. L., 2021, ApJ, 923, 65
Ferré-Mateu A., Trujillo I., Martín-Navarro I., Vazdekis A., Mezcua M., Balcells M., Domínguez L., 2017, MNRAS, 467, 1929
Gallazzi A., Charlot S., Brinchmann J., White S. D. M., Tremonti C. A., 2005, MNRAS, 362, 41

Gao Y. et al., 2018, ApJ, 869, 15
Harris C. R. et al., 2020, Nature, 585, 357
Hunter J. D., 2007, Comput. Sci. Eng., 9, 90
Iodice E. et al., 2016, ApJ, 820, 42
Karademir G. S., Remus R.-S., Burkert A., Dolag K., Hoffmann T. L., Moster B. P., Steinwandel U. P., Zhang J., 2019, MNRAS, 487, 318
Khochfar S. et al., 2011, MNRAS, 417, 845
Kroupa P., 2002, Science, 295, 82
Kroupa P., Jerabkova T., 2019, Nat. Astron., 3, 482
Lackner C. N., Cen R., Ostriker J. P., Joung M. R., 2012, MNRAS, 425, 641
La Barbera F., Ferreras I., Vazdekis A., de la Rosa I. G., de Carvalho R. R., Trevisan M., Falcón-Barroso J., Ricciardelli E., 2013, MNRAS, 433, 3017
La Barbera F., Vazdekis A., Ferreras I., Pasquali A., Cappellari M., Martín-Navarro I., Schönebeck F., Falcón-Barroso J., 2016, MNRAS, 457, 1468
La Barbera F. et al., 2019, MNRAS, 489, 4090
Li H. et al., 2017, ApJ, 838, 77
Lonoce I., Feldmeier-Krause A., Freedman W. L., 2021, ApJ, 920, 93
Lyubenova M. et al., 2016, MNRAS, 463, 3220
McConnell N. J., Lu J. R., Mann A. W., 2016, ApJ, 821, 39
McDermid R. M. et al., 2014, ApJ, 792, L37
McDermid R. M. et al., 2015, MNRAS, 448, 3484
Marks M., Kroupa P., Dabringhausen J., Pawlowski M. S., 2012, MNRAS, 422, 2246
Martín-Navarro I., Barbera F. L., Vazdekis A., Falcón-Barroso J., Ferreras I., 2015a, MNRAS, 447, 1033
Martín-Navarro I., La Barbera F., Vazdekis A., Ferré-Mateu A., Trujillo I., Beasley M. A., 2015b, MNRAS, 451, 1081
Martín-Navarro I. et al., 2015c, ApJ, 806, L31
Martín-Navarro I. et al., 2019, A&A, 626, A124
Martín-Navarro I. et al., 2021, A&A, 654, A59
Miller G. E., Scalo J. M., 1979, ApJS, 41, 513
Monachesi A. et al., 2019, MNRAS, 485, 2589
Nam D. G., Federrath C., Krumholz M. R., 2021, MNRAS, 503, 1138
Nipoti C., Cannarozzo C., Calura F., Sonnenfeld A., Treu T., 2020, MNRAS, 499, 559
Oldham L. J., Auger M. W., 2018, MNRAS, 474, 4169
Oser L., Ostriker J. P., Naab T., Johansson P. H., Burkert A., 2010, ApJ, 725, 2312
Parikh T. et al., 2018, MNRAS, 477, 3954
Perez F., Granger B. E., 2007, Comput. Sci. Eng., 9, 21
Pinna F. et al., 2019a, A&A, 623, A19
Pinna F. et al., 2019b, A&A, 625, A95
Poci A., McDermid R. M., Zhu L., van de Ven G., 2019, MNRAS, 487, 3776
Poci A. et al., 2021, A&A, 647, A145 (P21)
Posacki S., Cappellari M., Treu T., Pellegrini S., Ciotti L., 2015, MNRAS, 446, 493
Quenneville M. E., Liepold C. M., Ma C.-P., 2022, ApJ, 926, 30
Rodriguez-Gomez V. et al., 2016, MNRAS, 458, 2371
Rosani G., Pasquali A., La Barbera F., Ferreras I., Vazdekis A., 2018, MNRAS, 476, 5233
Salpeter E. E., 1955, ApJ, 121, 161
Sánchez-Blázquez P. et al., 2006, MNRAS, 371, 703
Sarzi M., Spiniello C., La Barbera F., Krajnović D., van den Bosch R., 2018, MNRAS, 478, 4084
Seabold S., Perktold J., 2010, in van der Walt S., Millman J., eds, Python in Science Conference, Austin, Texas, p. 92
Shetty S., Cappellari M., 2014, ApJ, 786, L10
Smith R. J., Alton P., Lucey J. R., Conroy C., Carter D., 2015, MNRAS, 454, L71
Sonnenfeld A., Treu T., Gavazzi R., Marshall P. J., Auger M. W., Suyu S. H., Koopmans L. V. E., Bolton A. S., 2012, ApJ, 752, 163
Spiniello C., Trager S., Koopmans L. V. E., Conroy C., 2014, MNRAS, 438, 1483
Spiniello C. et al., 2021, A&A, 646, A28
Thater S. et al., 2022, preprint (arXiv:2205.04165)
Thomas J. et al., 2011, MNRAS, 415, 545
Tortora C., Romanowsky A. J., Napolitano N. R., 2013, ApJ, 765, 8
Tortora C., La Barbera F., Napolitano N. R., Romanowsky A. J., Ferreras I., de Carvalho R. R., 2014, MNRAS, 445, 115
Tremonti C. A. et al., 2004, ApJ, 613, 898
Treu T., Auger M. W., Koopmans L. V. E., Gavazzi R., Marshall P. J., Bolton A. S., 2010, ApJ, 709, 1195
van de Ven G., De Zeeuw P. T., Van Den Bosch R. C. E., 2008, MNRAS, 385, 614
van den Bosch R. C. E., van de Ven G., Verolme E. K., Cappellari M., De Zeeuw P. T., 2008, MNRAS, 385, 647
van Dokkum P. G., Conroy C., 2012, ApJ, 760, 70
van Dokkum P., Conroy C., Villaume A., Brodie J., Romanowsky A. J., 2017, ApJ, 841, 68
Vaughan S. P., Davies R. L., Zieleniewski S., Houghton R. C. W., 2018, MNRAS, 479, 2443
Vazdekis A., Casuso E., Peletier R. F., Beckman J. E., 1996, ApJS, 106, 307
Vazdekis A., Koleva M., Ricciardelli E., Röck B., Falcón-Barroso J., 2016, MNRAS, 463, 3409
Venhola A. et al., 2018, A&A, 620, A165
Villaume A., Brodie J., Conroy C., Romanowsky A. J., van Dokkum P., 2017, ApJ, 850, L14
Virtanen P. et al., 2020, Nat. Methods, 17, 261
Wegner G. A., Corsini E. M., Thomas J., Saglia R. P., Bender R., Pu S. B., 2012, AJ, 144, 78
Yan Z., Jerabkova T., Kroupa P., 2020, A&A, 637, A68
Yan Z., Jeřábková T., Kroupa P., 2021, A&A, 655, A19
Zhu L. et al., 2018, MNRAS, 473, 3000
Zhu L. et al., 2020, MNRAS, 496, 1579

This paper has been typeset from a TEX/LATEX file prepared by the author.